

## SEMICONDUCTOR PLATE INTERACTING WITH $TE_{01}$ MODE IN CIRCULAR WAVEGUIDE

Ž. Kancleris, G. Šlekas, V. Tamošiūnas, R. Simniškis, P. Ragulis, and M. Tamošiūnienė

*Semiconductor Physics Institute, A. Goštauto 11, LT-01108 Vilnius, Lithuania*

E-mail: kancleris@pfi.lt

Received 24 December 2008; revised 20 February 2009; accepted 19 March 2009

In this paper, the possibility to use the semiconductor obstacle placed on the wall of the circular waveguide as the resistive sensor is analysed. The simplified model of the semiconductor obstacle is considered and the method to solve Maxwell's equations in the cylindrical coordinate system is presented for  $TE_{01}$  mode, which is most suitable for the transmission of high power signals. The finite-difference time-domain method was employed for the calculation of the electromagnetic field components in cylindrical waveguide, reflection coefficient from the semiconductor obstacle, and the average electric field in it. Computation results were tested by comparing computed results with the analytical solution.

**Keywords:** electromagnetic wave,  $TE_{01}$  mode, circular waveguide, semiconductor obstacle, resistive sensor

**PACS:** 41.20.-q, 07.50.-e

### 1. Introduction

Since the  $TE_{01}$  mode propagating in a circular waveguide is a low loss mode, it is often used for the design of microwave devices. The currents associated with  $TE_{01}$  modes are in the circumferential direction only and this property may be of some use to construct mode filters that suppress modes having currents directed along the waveguide axis [1]. The properties of  $TE_{01}$  mode mentioned above have been applied in [2–6].

The gyrotron-backward-wave-oscillator (gyro-BWO) experiments, which utilize a high-current (1–4 kA) and a high-voltage (300–500 keV) annular electron beam, were presented in [2]. The designed gyro-BWO operated in the  $TE_{01}$  backward wave mode, extracted power was 0.1–0.4 MW and cutoff frequency was approximately 4.2 GHz.

In [3], a design for circular waveguide bends propagating the low loss  $TE_{01}$  mode was considered. The detailed design of the bend and the comparison of simulation results with experimental data were presented. The bend has smooth walls and very low ohmic losses. The  $TE_{01}$  mode is transmitted with virtually perfect mode purity.

The theory for a single-time-switched resonant delay line pulse compression system has been developed in [4]. The switch operating in  $TE_{01}$  mode in a circular

waveguide avoiding the edge effects at the interface between the silicon wafer and the supporting waveguide was proposed. A design example for an active iris operating in  $TE_{01}$  mode has been presented.

The design and test of a 100 MW-band  $TE_{01}$  window was presented in [5]. A  $TE_{01}$  nonreciprocal phase shifter in a 50 MW test bench has been tested in [6].

The overview presented above confirms that circular waveguides operating at  $TE_{01}$  mode have been regularly used in high power microwave (HPM) experiments. In the present paper we have investigated the interaction of a semiconductor plate inserted into a circular waveguide with the  $TE_{01}$  mode propagating in it. We have solved Maxwell's equations using finite-difference time-domain (FDTD) method in a cylindrical coordinate system. The object of our investigation – the semiconductor plate – might be considered as a prototype of a resistive sensor (RS) [7]. The performance of it is based on electron heating effect and the RS is used for direct measurement of HPM pulses in the transmission lines and free space. The resistive sensors developed for rectangular waveguides are used in laboratories dealing with HPM pulses worldwide. Unfortunately, the RS for the circular waveguide has not been designed yet.

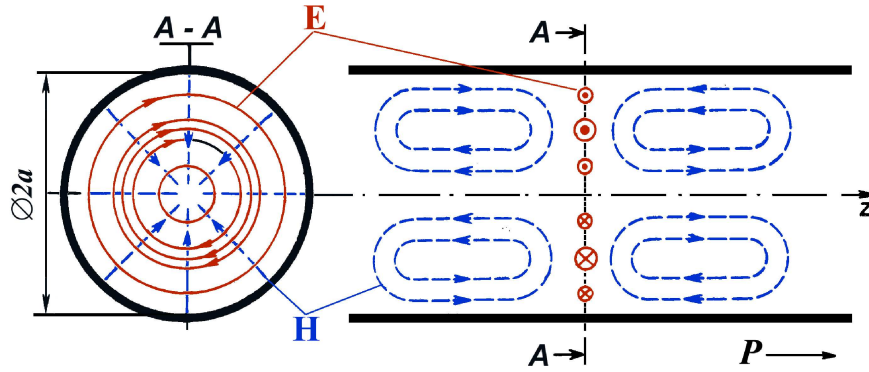


Fig. 1. The view of lines of the electromagnetic field in a circular waveguide for mode  $TE_{01}$ .

## 2. Electromagnetic field components

Although the  $TE_{01}$  mode is the simplest TE mode in the circular waveguide, it is not the lowest one. The critical frequency of the  $TE_{01}$  mode in a waveguide is twice that of the lowest  $TE_{11}$ . The view of lines of the electromagnetic field in the circular waveguide for mode  $TE_{01}$  is presented in Fig. 1. The regular wave has only three components:  $E_\varphi$ ,  $H_r$ , and  $H_z$ . They are independent of the azimuthal angle  $\varphi$ . Dependences of the amplitudes of the regular wave on the radial  $r$  and axial  $z$  coordinates can be expressed in the following way [8]:

$$E_\varphi(r, z) = A J_1\left(\frac{\mu_{01}r}{a}\right) \exp\left(-\frac{i2\pi z}{\lambda_w}\right), \quad (1)$$

$$H_r(r, z) = -A \frac{\lambda}{\lambda_w} \sqrt{\frac{\varepsilon_0}{\mu_0}} J_1\left(\frac{\mu_{01}r}{a}\right) \exp\left(-\frac{i2\pi z}{\lambda_w}\right), \quad (2)$$

$$H_z(r, z) = jA \frac{\lambda}{\lambda_c} \sqrt{\frac{\varepsilon_0}{\mu_0}} J_0\left(\frac{\mu_{01}r}{a}\right) \exp\left(-\frac{i2\pi z}{\lambda_w}\right). \quad (3)$$

Here the coefficient  $A$  is measured in electric field units and depends on the power propagating through the waveguide,  $\lambda$ ,  $\lambda_w$ , and  $\lambda_c$  are the wavelength of electromagnetic oscillations in free space, in a waveguide, and the critical wavelength for the  $TE_{01}$  mode, respectively,  $\varepsilon_0$  and  $\mu_0$  are the vacuum permittivity and permeability,  $J_0$  and  $J_1$  are the corresponding order first kind Bessel functions,  $\mu_{01} = 3.832$  is the root of  $J_1$ :  $J_1(\mu_{01}) = 0$ , and  $a$  is the radius of the waveguide. In the interval  $0-\mu_{01}$  Bessel function  $J_1$  reaches its maximum at  $\mu_{11} = 1.841$ , where  $\mu_{11}$  is the root of the first derivative of  $J_1$ . Therefore, the maximum of the components  $E_\varphi$  and  $H_r$  in the radial direction is almost halfway between the centre and the wall of the waveguide ( $r/a = \mu_{11}/\mu_{01} = 0.4804$ ).

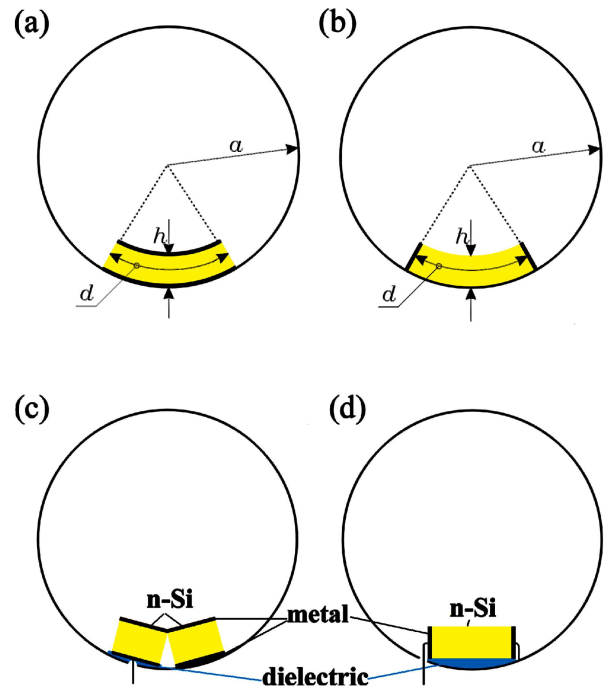


Fig. 2. A plate of the semiconductor with metal contacts on the wall of the circular waveguide: (a) contacts on the top and bottom surfaces – vertical configuration, (b) contacts on the sidewalls – horizontal configuration, and the practical realization of the (c) vertical and (d) horizontal configurations in the circular waveguide using plane samples.

The critical wavelength for the  $TE_{01}$  mode  $\lambda_c = 1.640a$  [8], and the wavelength in the waveguide is expressed as

$$\lambda_w = \frac{\lambda}{\sqrt{1 - (\lambda/\lambda_c)^2}}. \quad (4)$$

The power transfer by the  $TE_{01}$  mode can be straightforwardly computed by integrating the Poynting vector over cross-sectional area of the waveguide.

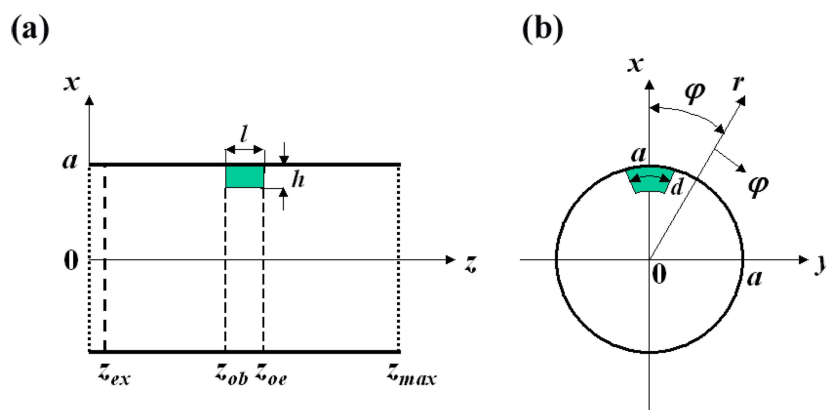


Fig. 3. Sectional view of the modelled circular waveguide with obstacle in (a)  $x0z$  plane and (b)  $x0y$  plane.

### 3. Layout of the sensing element

As already mentioned in Introduction, the performance of the RS is based on electron heating effect in semiconductors. Thus, the sensing element (SE) is actually a resistor made of  $n$ -type Si with two ohmic contacts. An electric field of electromagnetic wave heats electrons in the SE, its resistance increases, and by measuring this resistance change the pulse power of electromagnetic wave in the waveguide is determined [7]. Therefore, any plate inserted in the waveguide with properly arranged contacts could serve as a SE. Depending on the position of the metal contact on the plate, we propose two configurations shown in Fig. 2. We named “vertical” the plate with the contacts on its top and bottom, shown in Fig. 2(a), while a plate with the contacts on sidewalls was named “horizontal” (Fig. 2(b)). These two names will be used further without quotes to denote the particular configuration of the SE.

The possible practical realization of the vertical design using plane samples is shown in Fig. 2(c). It is seen that the proposed RS consists of two separate SEs placed in a close proximity to each other. Their top contacts are shorted with a thin metal foil. The bottom contact of one of the SEs is grounded while the other one is isolated from the waveguide and is used for the RS feeding and the output signal measurement. Actually, the sensing elements are connected in series with respect to the DC current but in parallel with respect to the microwave electric field.

The realization of the horizontal configuration is depicted in Fig. 2(d). It is seen that the plane SE is simply laid on the isolating dielectric on the wall of the waveguide. One of contacts of the SE is grounded, while the other one is isolated from the waveguide and is used for the RS feeding and the output signal measurement.

Comparing the vertical and horizontal configurations it can be concluded that, on the one hand, the vertical configuration can be simpler realized using the soldering technique for mounting of samples in the waveguide. It will not be the case for the horizontal configuration where the SE should be isolated from the wall of the waveguide. On the other hand, horizontal configuration might be more acceptable from the viewpoint of homogeneity of the electric field in the SE since the metal contacts are perpendicular to the direction of the electric field  $E_\varphi$  in the regular wave. In the vertical configuration, the contacts in general are parallel to the  $E_\varphi$ , therefore the regular component is zeroed by the contact surface.

### 4. FDTD method

For the calculation of electromagnetic field components in the waveguide with semiconductor obstacle we have used FDTD method [9, 10], application of which for cylindrical coordinate system will be given below.

The modelled section of the waveguide with the obstacle is shown in Fig. 3. We used a cylindrical coordinate system and dimensionless coordinates and time:  $r/a$ ,  $\varphi$ ,  $z/a$ ,  $tv/a$ , where  $v$  is the velocity of light in free space and  $a$  is a radius of the waveguide. In the plane  $z = z_{ex}$ , the  $TE_{01}$  type wave is excited. It propagates into both sides from the excitation plane. The obstacle is placed at one wavelength in the waveguide ahead from the excitation plane and at the same distance before the right side of the modelled waveguide section. In the planes  $z = 0$  and  $z = z_{max}$  nonreflecting boundary conditions are satisfied. Therefore, the waves travelling left from the excitation plane as well as reflected from the semiconductor obstacle are absorbed in the plane  $z = 0$ , whereas the wave passing semiconductor structure is absorbed in the plane

$z = z_{\max}$ . Due to the reflection from the semiconductor obstacle a partly standing wave is formed between planes  $z = z_{\text{ex}}$  and  $z = z_{\text{ob}}$ . From the amplitude distribution in this area, the reflection coefficient was determined.

Although the regular TE<sub>01</sub> type wave has one electric field component  $E_\varphi$  and two magnetic field components  $H_r$  and  $H_z$  (Eqs. (2) and (3)), in the vicinity of the SE all electromagnetic field components might appear. Therefore, to determine the average electric field amplitude in the semiconductor obstacle Maxwell's equations have to be solved computing all six components of the electric and magnetic fields. Making use of dimensionless variables and expressing the magnetic field strength in electric field units  $Z_0 H$ , where  $Z_0$  is an impedance of free space, Maxwell's equations in the semiconductor obstacle can be written down in a following way:

$$\frac{\partial \mathbf{E}}{\partial t} = \frac{\nabla \times \mathbf{H} - \gamma \mathbf{E}}{\varepsilon}, \quad (5)$$

$$\frac{\partial \mathbf{H}}{\partial t} = -\nabla \times \mathbf{E}, \quad (6)$$

where  $\gamma = Z_0 a / \rho$  accounts for losses in the structure. Here  $\rho$  and  $\varepsilon$  are the specific resistance and relative dielectric constant of the semiconductor obstacle and it is assumed that  $\mu = 1$  for the entire simulation area. Outside the semiconductor obstacle  $\gamma = 0$  and  $\varepsilon = 1$ .

Making use of cylindrical coordinates for the calculation of the curl of the electric and magnetic field and replacing time and coordinate derivatives in (5) and (6) with finite differences, one can obtain the following set of equations for updating new values of the components from the older ones:

$$\begin{aligned} H_r \Big|_{i,j+\frac{1}{2},k+\frac{1}{2}}^{n+\frac{1}{2}} &= H_r \Big|_{i,j+\frac{1}{2},k+\frac{1}{2}}^{n-\frac{1}{2}} + \frac{\Delta t}{\Delta z} \\ &\times \left( E_\varphi \Big|_{i,j+\frac{1}{2},k+1}^n - E_\varphi \Big|_{i,j+\frac{1}{2},k}^n \right) - \frac{\Delta t}{i\Delta\varphi\Delta r} \\ &\times \left( E_z \Big|_{i,j+1,k+\frac{1}{2}}^n - E_z \Big|_{i,j,k+\frac{1}{2}}^n \right), \end{aligned} \quad (7)$$

$$\begin{aligned} H_\varphi \Big|_{i+\frac{1}{2},j,k+\frac{1}{2}}^{n+\frac{1}{2}} &= H_\varphi \Big|_{i+\frac{1}{2},j,k+\frac{1}{2}}^{n-\frac{1}{2}} + \frac{\Delta t}{\Delta r} \\ &\times \left( E_z \Big|_{i+1,j,k+\frac{1}{2}}^n - E_z \Big|_{i,j,k+\frac{1}{2}}^n \right) - \frac{\Delta t}{\Delta z} \end{aligned}$$

$$\times \left( E_r \Big|_{i+\frac{1}{2},j,k+1}^n - E_r \Big|_{i+\frac{1}{2},j,k}^n \right), \quad (8)$$

$$\begin{aligned} H_z \Big|_{i+\frac{1}{2},j+\frac{1}{2},k}^{n+\frac{1}{2}} &= H_z \Big|_{i+\frac{1}{2},j+\frac{1}{2},k}^{n-\frac{1}{2}} + \frac{\Delta t}{(i+\frac{1}{2})\Delta r\Delta\varphi} \\ &\times \left( E_r \Big|_{i+\frac{1}{2},j+1,k}^n - E_r \Big|_{i+\frac{1}{2},j,k}^n \right) - \frac{\Delta t}{(i+\frac{1}{2})\Delta r} \\ &\times \left( (i+1)E_\varphi \Big|_{i+1,j+\frac{1}{2},k}^n - iE_\varphi \Big|_{i,j+\frac{1}{2},k}^n \right), \end{aligned} \quad (9)$$

$$\begin{aligned} E_r \Big|_{i+\frac{1}{2},j,k}^{n+1} &= E_r \Big|_{i+\frac{1}{2},j,k}^n + \frac{1}{\varepsilon} \left\{ -\gamma E_r \Big|_{i+\frac{1}{2},j,k}^n + \right. \\ &+ \frac{\Delta t}{(i+\frac{1}{2})\Delta r\Delta\varphi} \left( H_z \Big|_{i+\frac{1}{2},j+\frac{1}{2},k}^{n+\frac{1}{2}} - H_z \Big|_{i+\frac{1}{2},j-\frac{1}{2},k}^{n+\frac{1}{2}} \right) \\ &\left. - \frac{\Delta t}{\Delta z} \left( H_\varphi \Big|_{i+\frac{1}{2},j,k+\frac{1}{2}}^{n+\frac{1}{2}} - H_\varphi \Big|_{i+\frac{1}{2},j,k-\frac{1}{2}}^{n+\frac{1}{2}} \right) \right\}, \end{aligned} \quad (10)$$

$$\begin{aligned} E_\varphi \Big|_{i,j+\frac{1}{2},k}^{n+1} &= E_\varphi \Big|_{i,j+\frac{1}{2},k}^n + \frac{1}{\varepsilon} \left\{ -\gamma E_\varphi \Big|_{i,j+\frac{1}{2},k}^n + \right. \\ &+ \frac{\Delta t}{\Delta z} \left( H_r \Big|_{i,j+\frac{1}{2},k+\frac{1}{2}}^{n+\frac{1}{2}} - H_r \Big|_{i,j+\frac{1}{2},k-\frac{1}{2}}^{n+\frac{1}{2}} \right) \\ &\left. - \frac{\Delta t}{\Delta r} \left( H_z \Big|_{i+\frac{1}{2},j+\frac{1}{2},k}^{n+\frac{1}{2}} - H_z \Big|_{i-\frac{1}{2},j+\frac{1}{2},k}^{n+\frac{1}{2}} \right) \right\}, \end{aligned} \quad (11)$$

$$\begin{aligned} E_z \Big|_{i,j,k+\frac{1}{2}}^{n+1} &= E_z \Big|_{i,j,k+\frac{1}{2}}^n + \frac{1}{\varepsilon} \left\{ -\gamma E_z \Big|_{i,j,k+\frac{1}{2}}^n + \frac{\Delta t}{i\Delta r} \right. \\ &\times \left( (i+\frac{1}{2})H_\varphi \Big|_{i+\frac{1}{2},j,k+\frac{1}{2}}^{n+\frac{1}{2}} - (i-\frac{1}{2})H_\varphi \Big|_{i-\frac{1}{2},j,k+\frac{1}{2}}^{n+\frac{1}{2}} \right) \\ &\left. - \frac{\Delta t}{i\Delta\varphi\Delta r} \left( H_r \Big|_{i,j+\frac{1}{2},k+\frac{1}{2}}^{n+\frac{1}{2}} - H_r \Big|_{i,j-\frac{1}{2},k+\frac{1}{2}}^{n+\frac{1}{2}} \right) \right\}. \end{aligned} \quad (12)$$

In (7)–(12)  $\Delta t$ ,  $\Delta r$ ,  $\Delta\varphi$ , and  $\Delta z$  are time and cylindrical coordinate steps, lower indexes  $i$ ,  $j$ , and  $k$  stand for  $r$ ,  $\varphi$ , and  $z$ . The upper index  $n$  denotes the number of a time step. The grid of points where the particular component is computed is shifted at a half of step with respect to each other as it has been proposed by Yee [9]. Moreover, electric and magnetic fields are calculated at different time moments providing  $h^2$  accuracy in the calculation of both space and time derivatives. The details of the application of this technique

to the cylindrical coordinate system can be found in the monograph [10]. The grid can be chosen in such a way that it starts and finishes with the points where the electric field components should be calculated. For the investigated frequency range real metals can be sufficiently precisely simulated using so-called perfect electric conductor approximation, which assumes that tangential electric field components are simply zeroed on the metal surface. Therefore, the components  $E_\varphi$  and  $E_z$  are zeroed on the waveguide walls. Also, the grid has been chosen in such a way that tangential electromagnetic field components were located in the contact plane and consequently were zeroed during FDTD update. Depending on the considered configuration of the SE, corresponding components of the electric field are set to zero on the metal contacts:  $E_\varphi$  and  $E_z$  for the vertical configuration,  $E_r$  and  $E_z$  for the horizontal one. In the planes  $z = 0$  and  $z = z_{\max}$  nonreflecting boundary conditions for the components  $E_r$  and  $E_\varphi$  are satisfied.

At  $t \leq 0$  there are no electromagnetic fields in the modelled section of the waveguide, therefore all components of the electric and magnetic field are set to zero. When the dimensions of the semiconductor obstacle are much less than the characteristic dimensions of the waveguide, its influence on the wave propagating in the waveguide is comparatively small. In such a case, by filling the waveguide with the ordinary  $TE_{01}$  wave components, the stationary solution is achieved faster.

In choosing the time step, the Courant criterion formulated for 3D cylindrical coordinate FDTD procedure in [11] has to be taken into account. Considering the waveguide with the obstacle in an  $x0y$  (Fig. 3(b)) plane and having in mind that components of the regular  $TE_{01}$  wave are independent of  $\varphi$ , one can see that the distribution of electromagnetic field amplitudes should be symmetrical with respect to the  $x0z$  plane. Therefore, saving the computer memory only a half of the waveguide window is modelled.

Considering expressions for updating components of the electromagnetic field (7)–(12) it is seen that some of them, namely  $H_r$  (7),  $E_\varphi$  (11), and  $E_z$  (12) cannot be straightforwardly computed at  $i = 0$  ( $r = 0$ ). This fact is known as the numerical singularity of a FDTD scheme in cylindrical coordinates at  $r = 0$  [10]. A variety of numerical procedures dealing with the singularity has been proposed. More widely an integral form of Maxwell's equations near  $r = 0$  [12, 13] and the series polynomial expansion in the radial direction [14, 15] have been used to resolve the problem. We

have followed the simple method proposed in [16] and based on the use of the Cartesian coordinate system in the vicinity of  $r = 0$  leading to the following expressions for calculation of the components at  $i = 0$ :

$$H_r \Big|_{0, j+\frac{1}{2}, k+\frac{1}{2}}^{n+\frac{1}{2}} = \left( H_\varphi \Big|_{\frac{1}{2}, 0, k+\frac{1}{2}}^{n+\frac{1}{2}} - H_\varphi \Big|_{\frac{1}{2}, \pi, k+\frac{1}{2}}^{n+\frac{1}{2}} \right) \frac{\sin \varphi_{j+\frac{1}{2}}}{2} + \left( H_\varphi \Big|_{\frac{1}{2}, \frac{3\pi}{2}, k+\frac{1}{2}}^{n+\frac{1}{2}} - H_\varphi \Big|_{\frac{1}{2}, \frac{\pi}{2}, k+\frac{1}{2}}^{n+\frac{1}{2}} \right) \frac{\cos \varphi_{j+\frac{1}{2}}}{2}, \quad (13)$$

$$E_z \Big|_{0, j, k+\frac{1}{2}}^{n+1} = E_z \Big|_{0, j, k+\frac{1}{2}}^n + \frac{\Delta t}{\Delta r} \left( H_\varphi \Big|_{\frac{1}{2}, 0, k+\frac{1}{2}}^{n+\frac{1}{2}} + H_\varphi \Big|_{\frac{1}{2}, \frac{\pi}{2}, k+\frac{1}{2}}^{n+\frac{1}{2}} + H_\varphi \Big|_{\frac{1}{2}, \pi, k+\frac{1}{2}}^{n+\frac{1}{2}} + H_\varphi \Big|_{\frac{1}{2}, \frac{3\pi}{2}, k+\frac{1}{2}}^{n+\frac{1}{2}} \right), \quad (14)$$

$$E_\varphi \Big|_{0, j+\frac{1}{2}, k}^{n+1} = \left( E_r \Big|_{\frac{1}{2}, \pi, k}^{n+1} - E_r \Big|_{\frac{1}{2}, 0, k}^{n+1} \right) \frac{\sin \varphi_{j+\frac{1}{2}}}{2} + \left( E_r \Big|_{\frac{1}{2}, \frac{\pi}{2}, k}^{n+1} - E_r \Big|_{\frac{1}{2}, \frac{3\pi}{2}, k}^{n+1} \right) \frac{\cos \varphi_{j+\frac{1}{2}}}{2}, \quad (15)$$

where  $\varphi_{j+\frac{1}{2}} = (j + \frac{1}{2}) \Delta\varphi$ . The second index in  $H_\varphi$  and  $E_\varphi$  is formal, denoting the values of the component on the  $x$  or  $y$  axis. Thus, the components  $H_r$ ,  $E_z$ , and  $E_\varphi$  at  $r = 0$  can be straightforwardly computed using (13), (14), and (15). The only restriction is imposed on the azimuthal step  $\Delta\varphi$  size. It should be chosen as  $\pi/(2n)$ , where  $n = 1, 2, \dots$ .

## 5. The program

The program computing the electromagnetic field components was written using C++ programming language. It works as follows. During calculations the amplitudes of the particular component of the electromagnetic field at each point of the investigated structure are summed and stored in additional arrays. After each period, the amplitudes of the component  $E_\varphi$  are calculated. The values of  $E_\varphi$  for  $j = \frac{1}{2}$  and each  $i$  and  $k$  are compared with the values calculated one period earlier. The calculations are terminated when the largest difference between these values is less than the predetermined value  $\delta$ . Otherwise, the successive period is modelled. The number of periods that are necessary to model depends on the obstacle size and specific resistance. For small obstacles, the difference between amplitudes less than 0.01 can be achieved after 3 periods.

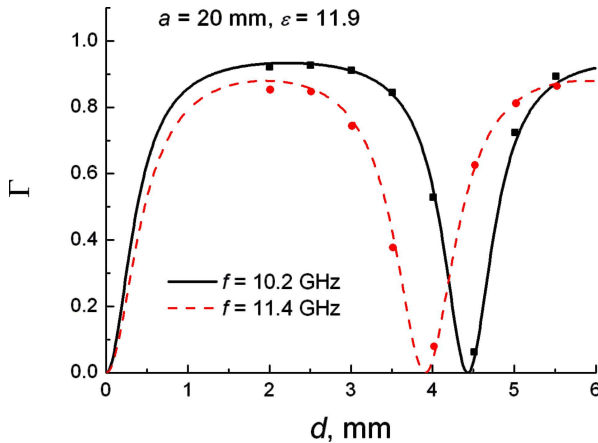


Fig. 4. Dependence of the reflection coefficient (power) on the width of the dielectric wafer. The wafer is inserted into circular waveguide, mode  $TE_{01}$ . Lines show analytical solution, points demonstrate calculation results of the FDTD modelling.

Calculations have been performed for the waveguide with the inner radius  $a = 2$  cm. For such waveguide the critical wavelength for the  $TE_{01}$  mode is  $\lambda_c = 3.28$  cm that corresponds to the cutoff frequency  $f_c = 9.14$  GHz. We performed calculations starting from  $f_c/f = 0.9$ ,  $f = 10.16$  GHz, towards higher frequencies. Typical dimensionless values of steps used in calculations were  $\Delta z = \Delta r = 0.025$ ,  $\Delta\varphi = 1.406^\circ$ ,  $\Delta t = 3 \cdot 10^{-4}$ , the value of the absolute error  $\delta$  was set to 0.01.

### 5.1. Comparison with analytical solution

Written program has been tested by comparing computed results with the analytical solution. The reflection coefficient from the width  $d$  dielectric wafer that is tightly inserted into the circular waveguide so that it fully covers its window was calculated. On the one hand, the reflection coefficient from such obstacle can be calculated using the program described above. On the other hand, it can be computed analytically considering a plane wave incident at angle  $\Theta$  from the normal to the dielectric plate of width  $d$ . For  $TE_{01}$  mode the wave with  $\mathbf{E}$  in the plane of incidence should be considered.

Calculation results obtained using our FDTD program and the analytical solution for two different frequencies are shown in Fig. 4. The radius of the waveguide, the relative dielectric constant and the electromagnetic wave frequency are given in the figure. It is seen that at some thickness of the wafer the Fabry–Pérot resonance conditions are fulfilled, the wafer brightens, and the reflection coefficient goes to zero. Good coincidence between the numerical results and

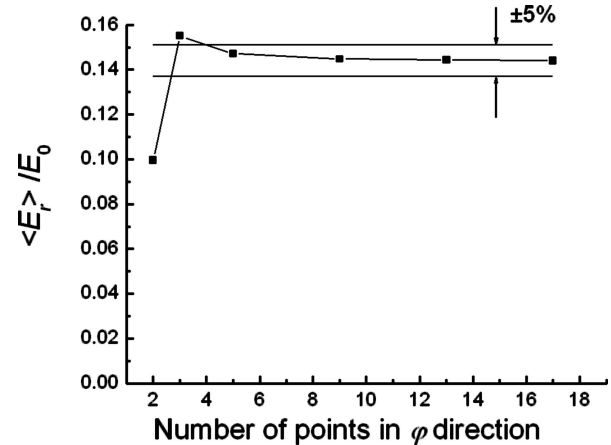


Fig. 5. Dependence of the average electric field in the obstacle on the number of points that are taken in the half of it in a transverse direction. Dimensions of the SE  $h \times d \times l = 2 \times 7.5 \times 4$  mm<sup>3</sup>, its specific resistance  $\rho = 20$   $\Omega$  cm, the radius of the waveguide  $a = 20$  mm, and frequency  $f = 11.4$  GHz.

analytical solution supports the validity of the FDTD program used in the calculations.

### 5.2. Number of points in the SE in transverse direction

From stability criterion of the FDTD solution in cylindrical coordinate system formulated in [11] it follows that while using fine meshes in both radial and azimuthal directions, the time step should be taken very short to provide stable solution. Therefore, when modelling the obstacle in the circular waveguide, it is very important to know how many points should be taken within it in  $\varphi$  direction to get an acceptable accuracy of the average electric field.

Results of the calculations of the average electric field in the SE for the different size of step  $\Delta\varphi$  are shown in Fig. 5. As usual, we modelled a half obstacle in the azimuthal direction. Consequently, the number of points denoted on the abscissa axis corresponds to a half obstacle. As one can see from the figure, 4–5 points in transverse direction is sufficient to get calculation accuracy within  $\pm 5\%$ .

## 6. Distribution of the electric field components within the SE

To have an idea about the electric field amplitudes in the obstacles of vertical and horizontal configurations an example of calculated distributions of the electric field components within the SE on different  $\varphi$ – $z$  surfaces are presented in Fig. 6. The calculations have been performed for the obstacle with dimensions  $h \times d \times l = 2 \times 4.6 \times 8$  mm<sup>3</sup> and specific resistance

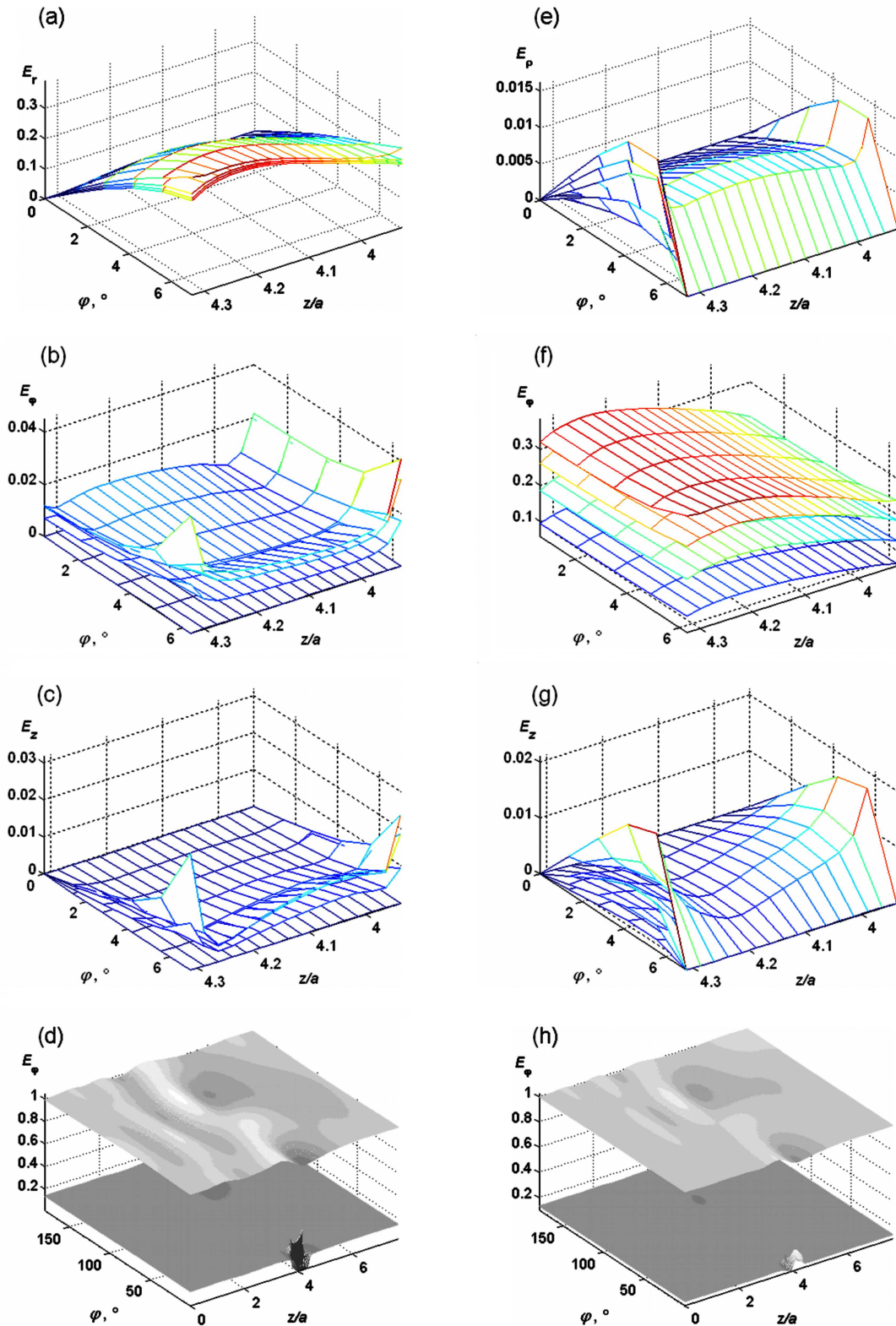


Fig. 6. Calculated distribution of the electric field components on a  $\varphi z$  surface for the semiconductor obstacle of  $\varepsilon = 11.9$  placed on the wall of the circular waveguide: (a), (b), and (c) within an obstacle in vertical configuration, (e), (f), and (g) in horizontal configuration, (d) and (h) in all modelled structure. Top distribution is on the surface where the amplitude  $E_\varphi$  is maximal in the regular  $TE_{01}$  wave, bottom distribution is on the surface that corresponds to the midpoint of the sample in  $r$  direction. Dimensions of the SE  $h \times d \times l = 2 \times 4.6 \times 8 \text{ mm}^3$ ,  $\rho = 20 \text{ } \Omega \text{ cm}$ ; the obstacle is modelled by  $4 \times 5 \times 16$  cells; frequency 10.2 GHz; waveguide radius 20 mm;  $\Delta r = \Delta z = 0.025$ ,  $\Delta \varphi = 1.4^\circ$ ,  $\Delta t = 3.05 \cdot 10^{-4}$ .

of 20  $\Omega$  cm. The SE was modelled by  $4 \times 5 \times 16$  cells, the frequency was 10.2 GHz, and the waveguide radius was 20 mm. Since the distribution of electric field components is symmetric, only a half of the SE is shown in the figures.

Although the electric field in the regular  $TE_{01}$  wave has the only component  $E_\varphi$ , in the obstacle  $E_r$  and  $E_z$  are also excited. As one can see from Fig. 6,  $E_r$  and  $E_z$  are zero in the symmetry plane ( $\varphi = 0$ ). Since the obstacle is symmetric with respect to the  $xOz$  plane, the waves propagating in the left and right side of the waveguide should also be symmetric. Therefore, the excited additional components, namely,  $E_r$ ,  $E_z$ , and  $H_\varphi$  should be antisymmetric:

$$E_r(t, r, \varphi, z) = -E_r(t, r, 360^\circ - \varphi, z), \quad (16)$$

and consequently in the symmetry plane they should be zero.

Although the electric field in the regular  $TE_{01}$  wave has the only component  $E_\varphi$ , the metal contact on the top of the SE in the vertical configuration effectively prevents the penetration of  $E_\varphi$  into the bulk of the obstacle. The main electrical component in the obstacle for this case is  $E_r$ . As already mentioned, this component is antisymmetric therefore it decreases to zero in the symmetry plane of the obstacle. As one can see from Fig. 6(a–c), the difference between electric field amplitudes on different surfaces is not so large. Closer to the upper contact the electric field amplitude slightly increases.

Considering electric field amplitude in the horizontal configuration (Fig. 6(e–g)) one can see that  $E_\varphi$  component, the only component in the regular  $TE_{01}$  wave, is the largest in the obstacle.  $E_r$  goes to zero at  $\varphi = 0$  due to symmetry (16) and approaches zero near the side wall of the obstacle due to a boundary condition for the tangential electric field near the metal surface. The same behaviour is characteristic of the component  $E_z$ .

One can notice that the averaged electric field in the obstacle mainly consists of a single component,  $E_r$  in vertical and  $E_\varphi$  in horizontal configuration, and the same order of magnitude of the averaged electric field is characteristic of the both configurations. The average amplitudes of the other two components are much less than the dominant one.

However, as one can see from the distributions of the components in all modelled space presented in (d) and (h) subplots of the figure, horizontal configuration of the sensor introduces a smaller perturbation of the electric field in the plane of maximal  $E_\varphi$  amplitude

and smaller amplitude of reflections. For this particular case VSWR introduced by the obstacle was 1.09 and 1.06 for the vertical and horizontal configuration, respectively. Such effect can be attributed to the orientation of the metal contacts with respect to the electric field of the incident wave. In general, the reflection from the obstacle is sufficiently small in both cases and the both configurations can be used as prototypes of the RS in the circular waveguide.

## 7. Conclusions

The peculiarities of interaction of the semiconductor obstacle placed on a wall of a circular waveguide with the mode  $TE_{01}$  have been investigated. Two different structures have been considered, with the contacts on top and bottom planes (vertical configuration) and with the contacts on sidewalls (horizontal configuration). A program based on the FDTD method was written, tested, and used for the calculation of the electromagnetic field components in cylindrical waveguide, reflection coefficient from the semiconductor obstacle, and the average electric field in it employing cylindrical coordinate system. The distribution of electric field components within the semiconductor obstacle placed on a wall of a circular waveguide and in all modelled structure has been calculated. The averaged electric field in the obstacle mainly consists of a single component,  $E_r$  in vertical and  $E_\varphi$  in horizontal configuration, and the same order of magnitude of the averaged electric field is characteristic of the both configurations. The average amplitudes of the other two components are much less than the dominant one. The reflection from the obstacle is sufficiently small in both cases and the both configurations can be used as prototypes of the RS in the circular waveguide. The model and program proposed here could be used for the calculation of the optimal sensors parameters.

## Acknowledgements

The work has been supported by the Air Force Office of Scientific Research, Air Force Material Command, USAF, under grant number FA8655-07-1-3028. Authors would like to acknowledge the partial support of this work by Directorate-General for Justice, Freedom and Security of the European Commission under the project “Assessment and mitigation of risk for disabling control centre of large power networks by intentional radiofrequency interference”.

## References

- [1] R. Chatterjee, *Elements of Microwave Engineering* (John Wiley & Sons, New York, Chichester, Brisbane, Toronto, 1986).
- [2] T.A. Spencer, C.E. Davis, K.J. Hendricks, F.J. Agee, and R.M. Gilgenbach, Results from gyrotron backward wave oscillator experiments utilizing a high-current high-voltage annular electron beam, *IEEE Trans. Plasma Sci.* **24**(3), 630–635 (1996).
- [3] S.G. Tantawi, A novel circular TE<sub>01</sub>-mode bend for ultra-high-power applications, *J. Electromag. Waves Appl.* **18**(12), 1679–1687 (2004).
- [4] S.G. Tantawi, R.D. Ruth, A.E. Vliexs, and M. Zolotarev, Active high-power RF pulse compression using optically switched resonant delay lines, *IEEE Trans. Microwave Theory Tech.* **45**(8), 1486–1492 (1997).
- [5] J. Neilson, L. Ives, and S.G. Tantawi, Design and test of a 100 MW-band TE<sub>01</sub> window, in: *Proceedings of the 2003 Particle Accelerator Conference*, (2003) p. 1125–1126.
- [6] J. Neilson and L. Ives, Development of a multi-megawatt circulator for X-band, in: *Proceedings of the 2003 Particle Accelerator Conference*, (2003) p. 1127.
- [7] M. Dagys, Ž. Kancleris, R. Simniškis, E. Schamiloglu, and F.J. Agee, Resistive sensor: Device for high-power microwave pulse measurement, *IEEE Antenn. Propag. Mag.* **43**(5), 64–79 (2001).
- [8] S.I. Baskakov, *Basics of Electrodynamics* (Soviet Radio, Moscow, 1973) [in Russian].
- [9] Kane S. Yee, Numerical solution of initial boundary value problems involving Maxwell's equation in isotropic media, *IEEE Trans. Antenn. Propag.* **14**(3), 302–307, (1966).
- [10] A. Taflove, *Computational Electrodynamics: The Finite-Difference Time-Domain Method* (Artech House, Norwood, MA, 1995).
- [11] Q. Chen and V. Fusco, Three dimensional cylindrical coordinate finite difference time domain analysis of curved slotline, in: *2nd International Conference on Computations in Electromagnetism*, Nottingham, U.K., May 13–15, 1994, pp. 323–326.
- [12] Y. Chen, R. Mittra, and P. Harms, Finite-difference time-domain algorithm for solving Maxwell's equation in rotationally symmetric geometries, *IEEE Trans. Microwave Theory Tech.* **44**(6), 832–839 (1996).
- [13] N. Dib, T. Weller, M. Scardeletti, and M. Imparato, Analysis of cylindrical transmission lines with the finite-difference time-domain method, *IEEE Trans. Microwave Theory Tech.* **47**(4), 509–512 (1999).
- [14] F. Liu and S. Crozier, An FDTD model for calculation of gradient-induced eddy currents in MRI system, *IEEE Trans. Appl. Supercond.* **14**(9), 1983–1989 (2004).
- [15] A. Trakic, H. Wang, F. Liu, H.S. López, and S. Crozier, Analysis of transient eddy currents in MRI using a cylindrical FDTD method, *IEEE Trans. Appl. Supercond.* **16**(3), 1924–1936 (2006).
- [16] Ž. Kancleris, Handling of singularity in finite-difference time-domain procedure for solving Maxwell's equations in cylindrical coordinate system, *IEEE Trans. Antenn. Propag.* **56**(2), 610–613 (2008).

## PUSLAIDININKINĖS PLOKŠTELĖS SAŲEIKA SU TE<sub>01</sub> MODA APVALIAJAME BANGOLAIDYJE

Ž. Kancleris, G. Šlekas, V. Tamošiūnas, R. Simniškis, P. Ragulis, M. Tamošiūnienė

*Puslaidininkų fizikos institutas, Vilnius, Lietuva*

### Santrauka

Apžvelgti TE<sub>01</sub> (H<sub>01</sub>) modos, sklindančios apvaliuoju bangolaidžiu, privalumai bei panaudojimas kuriant mikrobangų prietaisus. Išnagrinėta galimybė sukurti rezistorinį jutiklį, skirtą didelės galios mikrobangų impulsams matuoti, panaudojant puslaidininkinę kliūtį, esančią ant apvaliojo bangolaidžio sienelės. Pasiūlytos dvi jutiklio jautraus elemento realizacijos: vertikalioji, kai kontaktai yra sukurti ant viršutinio ir apatinio puslaidininkinės plokštelės paviršių, ir horizontalioji, kai metaliniai kontaktai suformuoti ant šoninių jutiklio plokštumų. Aptartos galimos praktinės jutiklių realizacijos, panaudojant plokščius jutiklius kaip jautriuosius elementus. Pasirinktas puslaidininkinės kliūties modelis ir pa-

teiktas Maksvelo lygčių cilindrinėje koordinatų sistemoje sprendimo metodas. Elektromagnetinio lauko sandų skaičiavimui buvo naudojamas baigtinių skirtumų laiko skalėje metodas. Aprašyta C++ programa, sukurta vidutiniam elektriniam laukui puslaidininkinėje kliūtyje ir atspindžio koeficientui nuo jo skaičiuoti. Sukurtos programos patikrintos lyginant skaičiavimo rezultatus su analiziniu sprendiniu. Apskaičiuotas elektrinio lauko pasiskirstymas vertikalios ir horizontalios konfigūracijos puslaidininkinėje kliūtyje, esančioje ant apvaliojo bangolaidžio vidinės sienelės, ir visame modeliuotame darinyje. Pasirodė, kad vertikalios konfigūracijos jutiklio viduje dominuoja  $E_r$  elektrinio lauko sandas, kai tuo tarpu horizontalios konfigūracijos jutiklyje didžiausias sandas yra  $E_\varphi$ .